Tunning of microstructure and thermoelectric properties of Ca3Co4O9 ceramics by high-magnetic-field sintering

Yanan Huang, Bangchuan Zhao, Jun Fang, Ran Ang, and Yuping Sun

Related Articles

Tailoring effective thermoelectric tensors and high-density power generation in a tubular Bi0.5Sb1.5Te3/Ni composite with cylindrical anisotropy
Appl. Phys. Lett. 101, 011906 (2012)

Enhancement of the thermoelectric properties in doped FeSb2 bulk crystals
J. Appl. Phys. 112, 013703 (2012)

Thermoelectric properties of FeGa3-type narrow-bandgap intermetallic compounds Ru(Ga,In)3: Experimental and calculational studies
J. Appl. Phys. 111, 123707 (2012)

Enhanced thermoelectric properties by Ir doping of PtSb2 with pyrite structure
Appl. Phys. Lett. 100, 252104 (2012)

An enhancement of a thermoelectric power factor in a Ga-doped ZnO system: A chemical compression by enlarged Ga solubility
Appl. Phys. Lett. 100, 253902 (2012)

Additional information on J. Appl. Phys.

Journal Homepage: http://jap.aip.org/

Journal Information: http://jap.aip.org/about/about_the_journal

Top downloads: http://jap.aip.org/features/most_downloaded

Information for Authors: http://jap.aip.org/authors

Tunning of microstructure and thermoelectric properties of $Ca_3Co_4O_9$ ceramics by high-magnetic-field sintering

Yanan Huang,[1] Bangchuan Zhao,[1,a)] Jun Fang,[2] Ran Ang,[1] and Yuping Sun[1,2]

[1]*Key Laboratory of Materials Physics, Institute of Solid State Physics, Chinese Academy of Sciences, Hefei 230031, People's Republic of China*
[2]*High Magnetic Field Laboratory, Chinese Academy of Sciences, Hefei 230031, People's Republic of China*

The structural, magnetic, electrical, and thermal transport properties of $Ca_3Co_4O_9$ ceramics sintered under high magnetic field were investigated. Crystal grain texturing and densification were achieved through cold-pressing and high-magnetic-field sintering techniques. The c-axis of the layered crystal grain was partly oriented along the c-axis of the pressed samples via a cold-pressing technique, and the degree of orientation was further increased while applying the magnetic field in the sample sintering progress. The easy magnetization axis of $Ca_3Co_4O_9$ polycrystalline ceramics was found to be the c-axis. The room-temperature resistivity along the ab-plane of the sample sintered under 8 T magnetic field was about 30% smaller than that of the sample sintered without magnetic field, and the Seebeck coefficient of the former reached 177.7 μV/K at the room temperature, which is about 50% larger than that of the latter. Consequently, for the sample sintered at 8 T magnetic field, the power factor along the ab-plane was enhanced by about 1.8 times compared to the sample without magnetic field sintering. The obtained result is suggested to originate from the variations of the carrier mobility and spin-orbital degeneracy due to high-magnetic-field sintering in the progress of the sample preparation. © *2011 American Institute of Physics*. [doi:10.1063/1.3671403]

I. INTRODUCTION

Since the discovery of high-temperature superconductivity in cuprates and colossal magnetoresistance in manganites, a great deal of interest has been generated regarding the study of $3d$ transition-metal oxides. Among these metal oxides, layered cobaltites with a quasi-two-dimensional triangular lattice, such as Na_xCoO_2 and $Ca_3Co_4O_9$, are more interesting due to their unusual thermoelectric (TE) properties.[1] TE materials need a high thermopower S and low resistivity ρ and thermal conductivity κ in order to exhibit a high figure of merit ZT ($=S^2/\rho\kappa$), which is usually used to characterize the performance of the TE material, and $ZT > 1$ is one of the criteria for the practical application of TE materials.[2,3] However, both thermopower and resistivity in the general material are functions of carrier concentration, and they can hardly be optimized at the same time. Layered cobaltites show a large room-temperature thermopower (larger than that of conventional metals) coexisting with a metallic-like electric conductivity and a very low thermal conductivity and have been widely considered as a potential candidate for TE materials,[3,4] especially in oxidizing atmospheres, due to their high chemical stability.

Layered oxide $Ca_3Co_4O_9$ can be denoted as $(Ca_2CoO_3)_{0.62}$ CoO_2 to acknowledge the incommensurate nature of the misfit structure, which is composed of an alternating stack along the c-axis of the CdI_2-type CoO_2 layers (first subsystem) and the rock salt (RS)-type CaO-CoO-CaO layers (second subsystem). Both subsystems have monoclinic crystal symmetry, with identical a, c, and β but different b parameters, and there exists structural misfit along the b-axis.[4–6] The CoO_2 subsystem, in which the two-dimensional triangular lattice of Co ions is formed by the network of edge-sharing CoO_2 octahedra, dominates the carrier transport and the electronic structure in the material.[7–9] The RS-type Ca_2CoO_3 layers can be regarded as the charge reservoir to supply charge carriers to the CoO_2 layers. The magnetic and transport properties of $Ca_3Co_4O_9$ cobaltite are quite complicated due to the misfit-layered structure. As for the transport properties, $Ca_3Co_4O_9$ undergoes an evolution with increasing temperature, from a low temperature insulator to a strongly correlated Fermi liquid at $\sim$80 K, to an incoherent metal, and finally to a semiconductor at elevated temperature.[10,11] At temperatures below $\sim$400 K, three magnetic transitions are observed—around $\sim$380 K, 27 K, and 19 K. The first magnetic transition, at $\sim$380 K, is suggested to be induced by the spin state transition.[1,9,10,12] With decreasing temperature, a short-range incommensurate spin-density-wave (IC-SDW) ordering appears below $\sim$100 K, whereas the long-range IC-SDW ordering is completed around $\sim$27 K, and the IC-SDW propagates within the ab-plane of the system. The formation of the IC-SDW is considered responsible for the metal-insulator (MI) transition around $\sim$80 K.[1,10,12] With further decreasing of the temperature, the system enters into a ferrimagnetic state (near $\sim$19 K). The low-temperature hysteresis loop shows that the ferrimagnetic interaction is parallel to the c-axis in the $Ca_3Co_4O_9$ system.[1,10,12] The majority carriers in $Ca_3Co_4O_9$ material are holes, as confirmed by Hall and thermopower measurements.

The mechanism of high TE performance in layered misfit cobaltites is quite different from that in conventional TE materials. The TE properties of conventional material can be understood by the band structure picture, whereas the high Seebeck coefficient in layered cobaltites is theoretically

a)Author to whom correspondence should be addressed. Electronic mail: bchzhao@issp.ac.cn. FAX: +86-551-559-1434.

explained in terms of the difference of the degrees of spin freedom of Co^{3+} and Co^{4+} ions in the CoO_2 layer. Therefore, the Seebeck coefficient and electric resistivity of the layered cobaltites can be controlled independently for the purpose of improvement of TE properties. In practice, different methods have been used to improve the TE properties in these layered cobaltites. One approach is to partially substitute some ions at Ca or Co sites in either RS or CO_2 layers so as to adjust the concentration of charge or spin in order to get high TE performance. For example, the ZT value of the $Ca_3Co_4O_9$ system can be improved by substituting Bi,[13] Ag,[14] and Lu (Ref. [15]) for Ca sites and transition metals[10] for Co sites. Due to the anisotropic properties of these oxides, another method for improving their TE properties is the fabrication of textured bulk materials with high crystal grain orientation. The well oriented samples exhibit an obvious increase in electrical conductivity relative to randomly oriented samples.[16] The decreasing resistivity is due to the higher texturing and the reduction of scattering for charge carriers at crystal grain boundaries or defects. The textured structure of these materials can be achieved through several means, such as the hot-forging technique, spark plasma sintering (SPS),[17] reactive templated grain growth, and magnetic alignment (MA).[18] Considering the magnetic anisotropic properties of these layered cobaltites, the MA is expected to be more effective for the formation of a textured structure in the whole bulk material than other methods. In order to further understand the effect of MA on the physical properties, especially the TE properties, of the $Ca_3Co_4O_9$ polycrystalline system, in this paper we carefully investigate the effect of cold-pressing and high-magnetic-field sintering techniques on the structural, magnetic, electrical transport, and thermoelectric characteristics in cobaltite $Ca_3Co_4O_9$ ceramics. Our results indicate that an applied high magnetic field in the sample fabrication progress can improve the electric conductivity and Seebeck coefficient, and thus the ZT values of the samples, simultaneously.

II. EXPERIMENTAL DETAILS

The target composition $Ca_3Co_4O_9$ was prepared using the citrate complexation sol-gel method. Stoichiometric amounts of high-purity $CaCO_3$ powders were dissolved in diluted nitric acid; this was followed by the addition of $Co(NO_3)_2 \cdot 6H_2O$ (in the appropriate stoichiometric ratio) dissolved in distilled water with continuous stirring, and then citric acid was added to make a solution complex. After all the reactants had been completely dissolved, the solution was heated on a hot plate, resulting in the formation of the gel. The gel was dried at $350\,^\circ C$ and then preheated at $650\,^\circ C$ in order to remove the remaining organics and decompose the nitrates in the gel. The obtained powders were fully grounded, pressed into circular tablets with a diameter of 10 mm and a thickness of 3 mm under a pressure of 20 MPa, and sintered at $800\,^\circ C$ for 5 h under applied magnetic fields of 0, 4, and 8 T. The direction of the applied magnetic field is perpendicular to the pressed surface of the $Ca_3Co_4O_9$ polycrystalline samples. In the following, we define the pressed surface of the sample as the ab-plane and the direction perpendicular to the surface as the c-axis for the $Ca_3Co_4O_9$ polycrystalline samples. According to this definition, the applied magnetic field is used parallel to the c-axis of the polycrystalline sample. We denote the $Ca_3Co_4O_9$ samples sintered under magnetic fields of 0, 4, and 8 T as the 0 T sample, the 4 T sample, and the 8 T sample, respectively.

The structure and phase purity of the samples were examined via powder x-ray diffraction (XRD) using a Philips X'pert PRO x-ray diffractometer with Cu K_α radiation and a scanning electron microscope (SEM) at room temperature. The magnetic properties of the studied samples were measured with the applied measuring magnetic field along the c-axis and ab-plane of the polycrystalline samples using a superconducting quantum interference device measurement system ($1.9\ K \leq T \leq 400\ K$, $0\ T \leq H \leq 5\ T$) in the temperature range of 5–350 K. The electrical and thermal transport properties were measured in a commercial Physical Property Measurement System ($1.8\ K \leq T \leq 400\ K$, $0\ T \leq H \leq 9\ T$). The conventional four-probe and two-probe methods were used for the in-plane and out-of-plane transport property measurements. All kinds of physical properties were measured twice in order to avoid occasional measuring errors.

III. RESULTS AND DISCUSSION

A. Textured microstructure

The XRD patterns for the ab-planes of the three $Ca_3Co_4O_9$ samples sintered under 0, 4, and 8 T fields at room temperature are shown in Fig. 1. The x-ray diffraction patterns of all studied samples are identical to the standard Joint Committee for Powder Diffraction Standards (JCPDS) card (21-0139) and the previously reported data for the $Ca_3Co_4O_9$ structure,[9] indicating the formation of single-phase compounds. Figure 1 shows that the cold-pressing and applied magnetic field sintering techniques do not change the lattice structure of the system. All x-ray peaks shown in Fig. 1 can be well indexed with a monoclinic lattice. In addition, x-ray diffraction of $Ca_3Co_4O_9$ ceramic bulks reveals strong peaks indexed as (00l), whereas the other diffraction
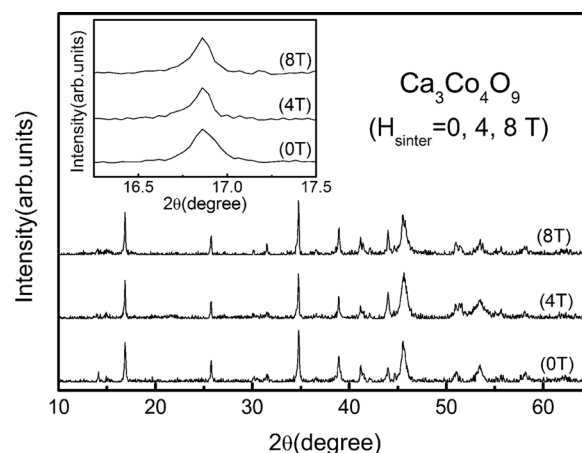

FIG. 1. XRD patterns for the ab-plane of $Ca_3Co_4O_9$ ceramics prepared under different applied sintering magnetic fields of 0, 4, and 8 T. The inset shows the change of the full width at half maximum of the enlarged (002) peaks due to variation of the applied sintering magnetic field.

TABLE I. Structural, magnetic, and thermoelectric transport properties of $Ca_3Co_4O_9$ ceramics sintered under applied sintering magnetic fields of 0, 4, and 8 T.

Parameter	0 T		4 T		8 T	
	c-axis	ab-plane	c-axis	ab-plane	c-axis	ab-plane
$P_{(00l)}$	0.97		1.03		1.07	
$F_{(00l)}$	0.89		0.93		0.97	
χ_{ab-5K} (10^{-4} emu g^{-1})	...	7.76	...	7.57	...	7.19
$\chi_{ab-300K}$ (10^{-4} emu g^{-1})	0.1093	0.1088	0.1130	0.1088	0.1145	0.1034
$\chi_{c-300K}/\chi_{ab-300K}$	1.0046		1.0386		1.1074	
M_r (emu/g)	1.26	1.05	1.28	1.07	1.37	0.99
H_c (kOe)	10.49	8.38	10.18	8.36	10.70	8.28
θ(K)	−104.0	−106.1	−119.4	−129.2	−119.5	−139.0
μ_{eff} (μ_B)	1.072	1.080	1.085	1.074	1.096	1.061
s	0.233	0.236	0.238	0.233	0.242	0.229
ρ_{300K} (10^{-2} Ω cm)	0.223	3.458	0.053	2.719	0.213	2.465
T_{min} (K)	99.9	93.9	93.9	92.8	95.9	89.9
T^* (K)	...	168.6	...	177.8	...	178.9
A (10^{-7} Ω/K)	...	2.18	...	1.73	...	1.71
γ (mJ mol^{-1} K^{-2})	121.6		120.6		109.3	
E_0 (meV)	...	1.942	...	1.898	...	1.869
T_0 (K)	...	1.976	...	1.960	...	1.030
T_{Smin} (K)	42.8	...	16.4	...	30.0	...
$S_{(300K)}$ (μV K^{-1})	113.6	125.2	124.8	133.8	121.2	177.7
$P_{(300K)}$ (μW m^{-1} K^{-2})	...	45.4	...	66.0	...	127.3
$\kappa_{ab-300K}$ (W K^{-1} m^{-1})	...	2.43	...	4.75	...	1.91
$\kappa_{ab-ch-300K}$ (W K^{-1} m^{-1})	...	0.254	...	0.200	...	0.181
ZT	...	0.00558	...	0.00414	...	0.0199

peaks are relatively weaker, which implies that the crystal grains grow along the c-axis of polycrystalline to form a highly textured structure.[19] The result shows that the textured structures can be obtained via the cold high-pressing method for the layered cobaltites as reported earlier.[25] In order to display the effect of applied sintering magnetic field on the $Ca_3Co_4O_9$ lattice, the enlarged (002) diffraction peaks of the studied samples are shown in the inset of Fig. 1. It displays clearly that the full width at half maximum of the peaks decreases for the samples sintered under applied magnetic field. This result might be related to variations of the orientation and size of crystal grains due to the applied high magnetic field in the sample sintering progress.

In order to check the effect of high-magnetic-field sintering on the textured structure quantitatively, the Lotgering factor F is used to evaluate the degree of crystal grain alignment.[20,21] The Lotgering factor is usually defined as

$$F = (P - P_0)/(1 - P_0), \qquad (1)$$

where $P = \Sigma I(00l)/\Sigma I(hkl)$ and $P_0 = \Sigma I_0(00l)/\Sigma I_0(hkl)$; P_0 can be calculated from the peak data of the JCPDS card. For a crystallographic isotropic (randomly oriented) sample, the value of P is P_0, i.e., $F = 0$, and for a c-axis direction completely aligned sample F is equal to 1. The relative ratio $P(00l)$ ($= \Sigma I(00l)/(\Sigma I(hkl) - \Sigma I(00l))$) of the peak intensity between (00l) peaks and the other peaks of the ab-plane are 0.97, 1.03, and 1.07 for the samples sintered under applied magnetic fields of 0, 4, and 8 T, and the calculated F values

are 0.89, 0.93, and 0.97, respectively, as listed in Table I. Obviously, the Lotgering factor value increases monotonously with increasing applied sintering magnetic field, implying that the crystal grain tends to rotate and the c-axis of the crystal grain aligns along the direction of the applied sintering magnetic field. The fact of the orientation of the crystal grains under the applied sintering magnetic field indicates that the c-axis is the easy magnetization axis for the $Ca_3Co_4O_9$ system.[22]

The textured structure of the studied samples can be further proved by the SEM micrographs. Figures 2(a)–2(c) illustrate the SEM images of the cross-section of $Ca_3Co_4O_9$ samples sintered under 0, 4, and 8 T magnetic fields, respectively. Plate-like crystal grains can be clearly observed in the figures; these are a result of the nature of the layered crystal structure of the $Ca_3Co_4O_9$ system.[21] In the samples sintered under applied magnetic field, the crystal grains become more homogeneous, smaller, and denser. Moreover, the c-axis of more plate-like crystal grains tends to array along the direction of the applied sintering magnetic field, indicating that the textured structure becomes clearer for the samples sintered under applied magnetic field.

Figure 2(d) shows the SEM image of the ab-plane for the 0 T sample. From Figs. 2(a) and 2(d) we can see that the 0 T sample already shows a relatively highly textured structure. The c-axis of the crystal grains in the sample is preferred to align along the pressing direction after being compacted under high pressure and then subjected to sintering treatment. For these misfit layered cobaltites, high quality ceramic samples
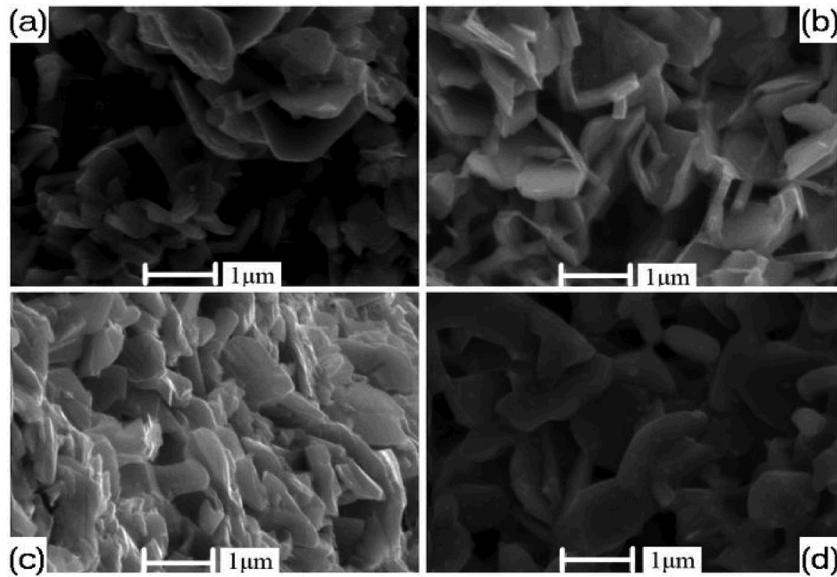
FIG. 2. SEM micrographs for (a)–(c) the cross-section of $Ca_3Co_4O_9$ ceramics with different applied sintering magnetic fields from 0 T to 8 T in the parallel direction and (d) the ab-plane of the 0 T $Ca_3Co_4O_9$ ceramics in the vertical direction.

with a large crystallographic anisotropy can be fabricated via the simple cold high-pressure method.[2] With increasing sample sintering magnetic field, the arrangement of crystal grains becomes denser and more ordered, and the degree of crystal grain orientation increases monotonously. That is to say, a textured $Ca_3Co_4O_9$ ceramic can be obtained via the cold-pressure method, and the degree of texturing becomes higher when the samples are sintered under high magnetic field. The result shows that the MA is an effective way to control the microstructure of layered polycrystalline cobaltites, and thus to improve the TE properties of the samples.[18,23] This result is consistent with that of XRD analysis, as aforementioned. Compared with $Ca_3Co_4O_9$ ceramics synthesized via template growth or hot-pressure methods,[24] the present studied samples have a relatively large density and degree of texturing, and the grain size is homogeneous and small.[2]

B. Magnetic properties

The magnetic measurements of the $Ca_3Co_4O_9$ samples were performed in the field-cooling (FC) mode under an applied measuring magnetic field of 0.1 T in the wide temperature range of 5–350 K. For the magnetic measurements, the applied measuring magnetic field was parallel to the ab-plane of the polycrystalline samples (defined as χ_{ab}). The dc in-plane susceptibility χ_{ab} as a function of temperature for the 0 T sample is shown in Fig. 3 as an example. The samples sintered under high magnetic field show a temperature dependence of susceptibility behavior in the whole studied temperature range similar to that of the 0 T sample: the susceptibility increases slowly with decreasing temperature to $\sim$25 K. As the temperature decreases further, the susceptibility increases observably; this effect is suggested to originate from ferrimagnetic transition.[1,7] The obtained result is consistent with that reported in Ref. 1. Moreover, the low-temperature in-plane susceptibility of the samples decreases, and the sudden raise becomes mild slowly as the sintering magnetic field increases from 0 to 8 T. The magnitudes of the in-plane susceptibilities at 5 K χ_{ab-5K} are listed in Table I for all samples. The result shows that the low-temperature

in-plane ferrimagnetic transition can be suppressed by the applied magnetic field in the sample sintering progress.

The temperature dependence of the FC magnetic susceptibility was also measured with the applied measuring field perpendicular to the pressed surface (χ_c), and the result for the 0 T sample is also shown in Fig. 3 as an example. For the 0 T sample, the value of χ_c is slightly larger than that of χ_{ab}. Both room-temperature χ_c and χ_{ab} are also listed in Table I. It can be seen that magnetic anisotropy exists between χ_{ab} and χ_c. Moreover, the low-temperature $\chi_{ab}(T)$ upturn is milder than that of the c-axis, implying that the ferrimagnetic interaction mainly occurs between the RS and CoO_2 layers and the magnetic anisotropy has already been formed by the cold-pressing technique. The result can be further proved by the isothermal magnetic measurement $M(H)$ at 5 K and the values of the residual magnetization M_r and the coercive field H_c, as shown in Fig. 4 and Table I.

Next, we show the anisotropic property quantitatively, and the temperature dependence of the ratio of FC susceptibilities χ_c/χ_{ab} between χ_c and χ_{ab} is plotted in Fig. 5. Figure 5 indicates that χ_c/χ_{ab} of each specific sample almost stays
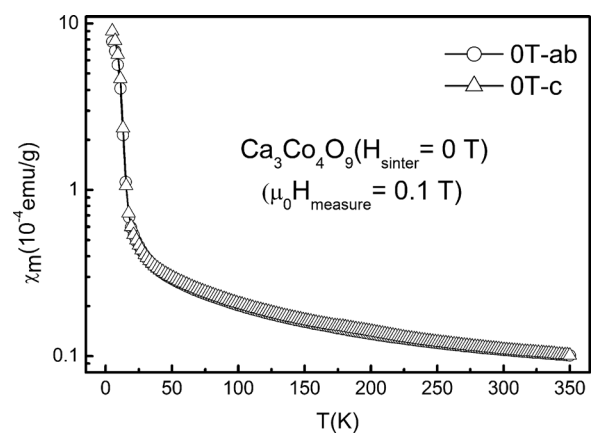

FIG. 3. Temperature dependence of FC susceptibilities (χ) in the field-cooling mode under an applied measuring magnetic field of 0.1 T in a wide temperature range of 5–350 K for the ab-plane and the c-axis of the 0 T sample as an example.
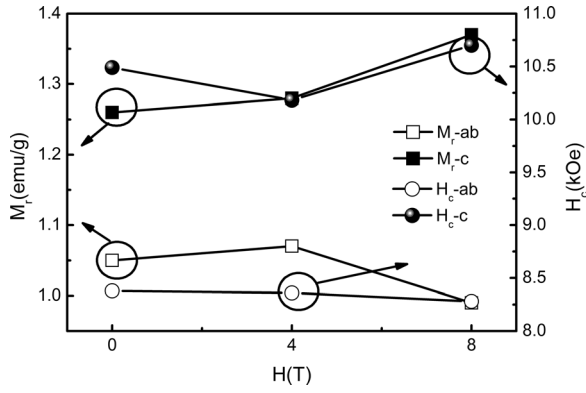
FIG. 4. Sintering magnetic field dependences of the residual magnetization M_r and the coercive field H_c at 5 K for the ab-plane and the c-axis of all three samples.

constant in the high temperature range above $\sim$25 K. As the temperature decreases from 25 K, the value of χ_c/χ_{ab} increases abruptly; this is suggested to be related to the formation of the long-range IC-SDW state and the ferrimagnetic transition as aforementioned. Figure 5 displays that with increasing applied magnetic field in the sample sintering progress from 0 T to 8 T, the magnitude of χ_c/χ_{ab} increases monotonously in the whole studied temperature range, and the room-temperature values of χ_c/χ_{ab} are listed in Table I for all samples, implying that the applied magnetic field in the sample sintering process might be in favor of the showing of the anisotropic magnetic property of $Ca_3Co_4O_9$ polycrystalline samples due to the increasing degree of texture of crystal grains, as shown in XRD and SEM measurements (see Figs. 1 and 2). In addition, $\chi_c/\chi_{ab} > 1$ also reflects the fact that the c-axis is the easy magnetization axis for $Ca_3Co_4O_9$ system. Therefore, in the sample fabrication progress, the application of high magnetic field is an effective approach for controlling the microstructure and the anisotropic magnetic properties of layered cobalt oxide materials.[18,23] The improved magnetic anisotropy is an important ingredient for modifying the TE properties of $Ca_3Co_4O_9$ polycrystalline samples, as discussed below.

In order to analyze quantitatively the effect of the sintering magnetic field on the magnetic properties of the samples, we try to fit the temperature dependence of the inverse sus-
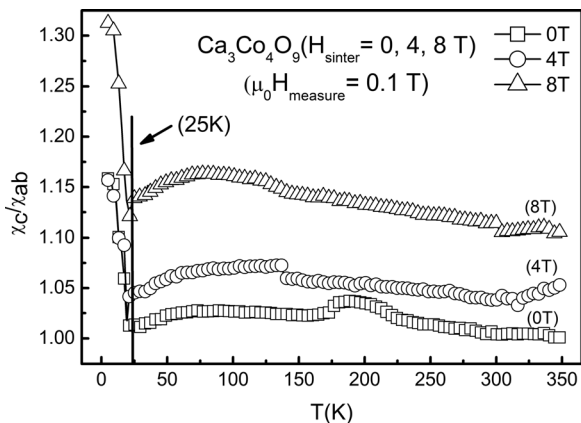

FIG. 5. Temperature dependence of the ratios of the FC susceptibilities (χ) between the c-axis and the ab-plane for all three samples, denoted as χ_c/χ_{ab}.

ceptibility, i.e., $\chi^{-1}(T)$, according to the Curie-Weiss law. It is observed that all $\chi^{-1}(T)$ curves (including ab-plane and c-axis) follow the Curie-Weiss law well above $\sim$50 K. $\chi^{-1}(T)$ decreases almost linearly with decreasing temperature to about $\sim$50 K, and then it sharply decreases as the temperature decreases further near about $\sim$19 K. The anomaly near $\sim$19 K in the $\chi^{-1}(T)$ curve is suggested to originate from the ferrimagnetic transition, as reported earlier.[1,7] By fitting the $\chi^{-1}(T)$ curve in the high temperature range above 50 K according to the Curie-Weiss law,

$$\chi^{-1}(T) = 3k_B(T - \theta)N_0^{-1}\mu_{eff}^{-2}, \quad (2)$$

where k_B, T, θ, N_0, and μ_{eff} are the Boltzmann constant, the absolute temperature, the Weiss temperature, Avogadro's constant, and the effective magnetic moment, respectively;[5,25] the values of θ and μ_{eff} have been obtained and are listed in Table I.

Table I shows that the Weiss constants θ of all studied samples are negative, and the absolute value of θ increases with increasing sample sintering field. The negative value of θ indicates the presence of ferrimagnetic interaction in the studied samples at low temperatures, and the ferrimagnetism decreases in the samples sintered under high magnetic field,[10] which induces a small reduction of the susceptibility of the samples. This result is consistent with that of the low-temperature magnetic susceptibility analysis discussed above. Moreover, the values of θ obtained from the $\chi_{ab}^{-1}(T)$ curve for all the samples are smaller than that of the c-axis magnetic susceptibility curve, and the difference between the two θ values increases significantly with increasing sample sintering magnetic field. The effective magnetic moment μ_{eff} also exhibits an obvious anisotropic property. The value of μ_{eff} obtained from the ab-plane susceptibility for the 0 T sample is somewhat larger than that obtained from the c-axis susceptibility. It is interesting that with increasing sample sintering magnetic field, μ_{eff} of the c-axis increases, whereas μ_{eff} of the ab-plane decreases, and then the anisotropic magnetic property of the studied samples is enhanced. The spin quantum number s was calculated based on the value of μ_{eff}, and the calculated results are also shown in Table I. It shows that the values of s obtained from both the ab-plane and the c-axis susceptibility are consistent with those reported earlier. The enhanced magnetic anisotropy might be related to the grain orientation under high magnetic field in the sample sintering progress. As reported previously, there exist complex magnetic interactions in the $Ca_3Co_4O_9$ system. The ferrimagnetism in the system is mainly caused by the interlayer coupling between CoO_2 and Ca_2CoO_3 subsystems. In addition, superexchange and double exchange interactions between Co^{3+} and Co^{4+} ions coexist in the CoO_2 layers,[1,9,10,12] and the variable spin states of Co ions exist simultaneously to make spin states more complex and to induce more rich physical properties in the system. In a single $Ca_3Co_4O_9$ crystal grain, the c-axis susceptibility is always somewhat larger than that of the ab-plane. From the SEM analysis, most of the crystal grains in the 0 T sample appear to array randomly, and the c-axis of partial crystal grains tends to be frozen instantly by the instant cold-pressing (20 MPa) and aligns along the ab-plane

of the polycrystalline sample, which results in the μ_{eff} of the ab-plane for the 0 T sample being larger than that of the c-axis. When the sintering magnetic field is applied, the c-axis of the partial crystal grains in the sample tends to align along the applied sample sintering magnetic field. When the sample is sintered under high magnetic field, the c-axis of most single $Ca_3Co_4O_9$ crystal grains is aligned along the c-axis of the polycrystalline sample to form a highly textured structure. As a result, the c-axis and ab-plane effective magnetic moments have contrary change trends under the applied sintering magnetic field, and thus the μ_{eff} along the c-axis of a polycrystalline sample sintered under applied magnetic field is larger than that along the ab-plane due to the change of orientation of partial crystal grains.

In order to study the magnetic structure of the present samples in depth, we plot the low temperature $d\chi^{-1}(T)/dT$ versus T curve for the c-axis of the 0 T sample as an example in Fig. 6. Interestingly, there exists a small shoulder in the $d\chi^{-1}(T)/dT$ versus T curves at about $\sim$27 K for all samples, as highlighted in the circled region in Fig. 6. It should be noted that such a magnetic shoulder can be observed only in $Ca_3Co_4O_9$ single crystal, as reported earlier,[26,27] and no obvious magnetic shoulder has been observed in $Ca_3Co_4O_9$ polycrystalline samples. The magnetic shoulder in the $d\chi^{-1}(T)/dT$ curve for the single crystal sample is suggested to originate from the completion of the spin-density-wave (SDW) transition, which has already been detected by the muon spin rotation and relaxation measurement.[1,12,26] Therefore, we can also ascribe the anomaly in the $d\chi^{-1}(T)/dT$ versus T curve near $\sim$27 K in the present samples to the completion of the SDW transition. Considering the similarity of the single crystal and present studied samples, we can conclude that the SDW state can appear in samples with a layered structure.[26] For the $Ca_3Co_4O_9$ polycrystalline sample reported earlier, the change in $d\chi^{-1}(T)/dT$ at the SDW transition temperature T_{SDW} is expected to be small and anisotropic due to its broad transition width and two dimensional structure, and such a shoulder will be difficult to detect.[26,27] Therefore, it is plausible that the cold-pressure method and the magneto-scientific approach are effective in controlling

the microstructure of the polycrystalline samples, and thus the magnetic properties of the layered cobaltite $Ca_3Co_4O_9$ system,[18,23] which is consistent with the aforementioned results of the XRD and SEM measurements. For the 0 T sample, the shoulder in the $d\chi_c^{-1}(T)/dT$ versus T curve is more pronounced than that observed in the ab-plane curve, which is close to that of $Ca_3Co_4O_9$ single crystal. With increasing sample sintering magnetic field, the magnetic shoulders in both the c-axis and the ab-plane curves decrease, and the shoulder in the c-axis magnetic curve decreases more quickly. This result shows that the applied magnetic field in the sample sintering progress might suppress the SDW transition in layered cobaltites and the SDW propagates within the ab-plane of the system.

C. Electric transport property

The temperature dependence of the resistivity of all the three studied samples was measured under zero measuring magnetic field in the temperature range of 2–350 K using a standard four terminal method. For the resistivity measurement, the electric current flows through the pressed surface (i.e., the in-plane resistivity ρ_{ab}) and the cross-section (i.e., the out-of-plane resistivity ρ_c) of the pressed polycrystalline sample. Figure 7 shows the temperature dependence of the in-plane resistivity ρ_{ab} for all samples. It shows that the ρ_{ab} curves for all samples show a metallic-like behavior ($d\rho_{ab}/dT > 0$) in the high-temperature range above T_{min} and semiconducting-like transport behavior ($d\rho_{ab}/dT < 0$) below T_{min}. That is to say, there exists a metal-insulator transition in the $\rho_{ab}(T)$ curves for all samples at T_{min}. The temperature dependence of the $\rho_{ab}(T)$ here is quite similar to that of a single crystal as reported earlier.[11] With increasing sample sintering magnetic field, the value of $\rho_{ab}(T)$ decreases monotonously. The magnitude of the room-temperature resistivity $\rho_{ab-300K}$ decreases from 34.58 mΩ cm for the 0 T sample to 24.65 mΩ cm for the 8 T sample, as listed in Table I, along with that of the out-of-plane room-temperature resistivity ρ_c. The decrease in resistivity might be related to the
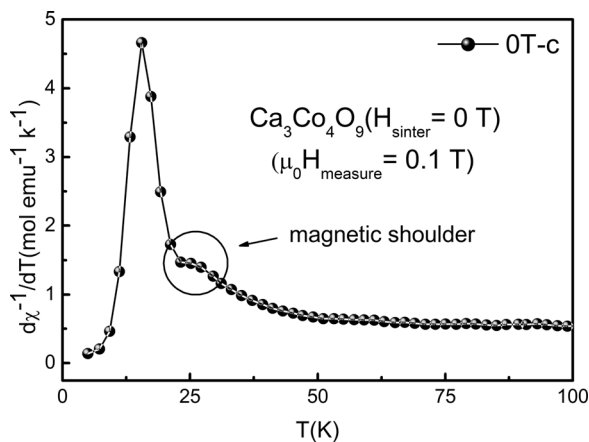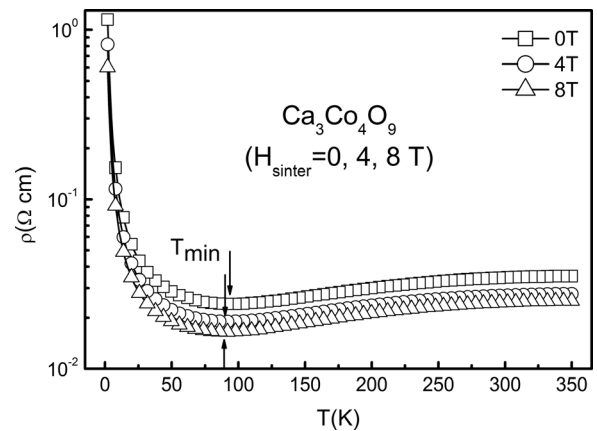

FIG. 6. Curve of $d\chi^{-1}/dT$ vs T for the c-axis of the 0 T sample. The shoulder is shown in the circled region of the $d\chi^{-1}/dT$ curve in the temperature range of 20–34 K.

FIG. 7. Temperature dependence of the in-plane resistivity $\rho_{ab}(T)$ for the $Ca_3Co_4O_9$ samples (H_{sinter} = 0, 4, 8 T) measured under zero magnetic field in the temperature range of 2–350 K using a standard four terminal method. Here, T_{min} is a transition temperature between metal-like behavior ($d\rho_{ab}/dT > 0$) above T_{min} and semiconducting-like behavior ($d\rho_{ab}/dT < 0$) below T_{min}.

crystal grain texturing and densification under the high-magnetic-field sintering, which would induce an increase of the carrier mobility μ within the ab-plane of the samples. According to the results of the SEM measurements as aforementioned, the crystal grains become more homogeneous, smaller, and denser, and the c-axis of the crystal grain tends to align along the direction of the applied sintering field. Then the scattering at grain boundaries along the ab-plane decreases and the mobility of the carriers increases in the samples fabricated under high magnetic field, resulting in a decrease of the grain boundary resistance. However, the applied sintering magnetic field does not change the carrier concentration of single crystal grains, and the intragranular resistance is unchanged. Thus, the conductivity of the samples increases with increasing applied magnetic field in the sample sintering progress. All the samples have similar temperature dependent behavior for the out-of-plane resistivity $\rho_c(T)$ and that of $\rho_{ab}(T)$ in the studied temperature range (not shown here).

Now we pay attention to the metal-insulator transition at T_{min} in the $\rho_{ab}(T)$ curve. From Fig. 7, we can see that T_{min} shifts to a lower temperature range slowly as the applied magnetic field increases in the sample fabrication process. T_{min} decreases from 93.9 K for the 0 T sample to 89.9 K for the 8 T sample, and the values of T_{min} are listed in Table I. Here, T_{min} is defined as the temperature at which the slope $d\rho(T)/dT$ is zero in the $\rho_{ab}(T)$ curves. The MI transition at T_{min} in the $Ca_3Co_4O_9$ system is always considered as related to the localization of charge carriers caused by the IC-SDW state.[1,7,22] As discussed above, the applied magnetic field in the sample fabrication progress plays a negative role in the formation of the SDW state. Therefore the localization of the carriers is weaker and the carrier mobility becomes larger in the samples sintered under applied magnetic field, resulting in a smaller T_{min}.

As reported previously,[9,28] the temperature dependence of the resistivity of $Ca_3Co_4O_9$ samples in a wide temperature range can be distinguished as four transport regimes. In the low-temperature range, below T_{min}, $\rho_{ab}(T)$ behaves as an insulator characterized by a negative slope of the curve. As the temperature increases, the $\rho_{ab}(T)$ curve exhibits metallic behavior with two regimes, which can be identified as a strongly correlated Fermi-liquid regime up to the temperature T^* (~ 168.6 K for a pure $Ca_3Co_4O_9$ sample) and then an incoherent metal regime. With the temperature increasing further, the $Ca_3Co_4O_9$ sample finally undergoes a semiconductor at elevated temperatures.[10,11] As aforementioned,[10] there exist two characteristic temperatures in the $\rho_{ab}(T)$ curve of the $Ca_3Co_4O_9$ system between 5 and 300 K, T_{min} and T^*, where T_{min} is the MI transition temperature and T^* is the transition temperature from Fermi liquid to an incoherent metal.[29]

In general, the transport behavior of a Fermi liquid system can be described with the following equation:

$$\rho = \rho_0 + AT^2, \tag{3}$$

where ρ_0 is the residual resistivity due to the domain boundaries and other temperature-independent scattering mechanisms,[30] and A is the Fermi liquid transport coefficient;[10]
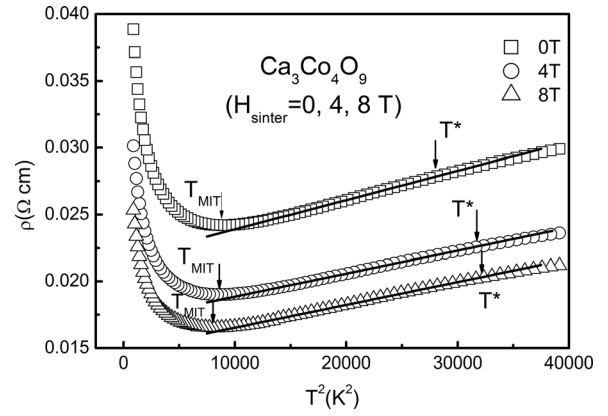

FIG. 8. Plot of $\rho_{ab}(T)$ vs T^2 with fitted lines for the $Ca_3Co_4O_9$ samples with $H_{sinter} = 0$, 4, and 8 T, measured under zero magnetic field in the temperature range of 2–200 K. T_{min} is the MI transition temperature and T^* is the transition temperature from Fermi liquid to incoherent metal.

AT^2 reflects the electron-electron scattering mechanisms of carriers. In order to obtain the effect of the applied sintering magnetic field on the transport properties of the $Ca_3Co_4O_9$ system, we try to fit the $\rho_{ab}(T)$ curve in the metallic range just above T_{min} using Eq. (3), and the fitting results are shown in Fig. 8. It can be seen that the temperature region in which the $\rho_{ab}(T)$ can be well fitted by Eq. (3) becomes wider under the applied magnetic field, implying that the temperature region of electron-electron scattering becomes wider. In order to clarify, the values of T_{min} and T^*, along with the fitting parameter A, are also listed in Table I. Here, T^* is defined as the end temperature of the linear dependence for $\rho \sim T^2$.[2,10] As the sample sintering magnetic field increases, the parameter A decreases while T^* increases. According to the dynamical mean field theory,[10,31] a key role of the effective mass m^* of a Fermi liquid is predicted as $T^* \sim 1/m^*$ and $A \sim (m^*)$.[2] The increase of T^* and the decrease of A indicate the decrease of m^* under the applied magnetic field. The notable decrease of m^* in the samples sintered under high magnetic field implies an increased bandwidth and a weakened electronic correlation in these compounds.[10]

In order to further study the effect of the applied magnetic field on m^* and electronic correlation, specific heat measurements were also performed.[10] The temperature dependence of the specific heat C for the 0 T sample in the low-temperature range is plotted in the main panel of Fig. 9 as an example. In general, the specific heat of a sample can be written as

$$C = \gamma T + \beta T^3, \tag{4}$$

where γ is the electronic specific heat coefficient and β is the lattice specific heat coefficient;[20] γT and βT^3 denote the electron and lattice contributions to the specific heat, respectively. As shown in the inset of Fig. 9, where the figure is plotted as $C(T)/T$ versus T^2, an obvious Schottky anomaly appears in the low-temperature range. Considering the minor contribution of the Schottky anomaly to the specific heat in the temperature range above the Schottky temperature in misfit cobalt oxide, the direct determination of γ from the linear T^2 behavior of the $C(T)/T$ curve over a sizable temperature interval is
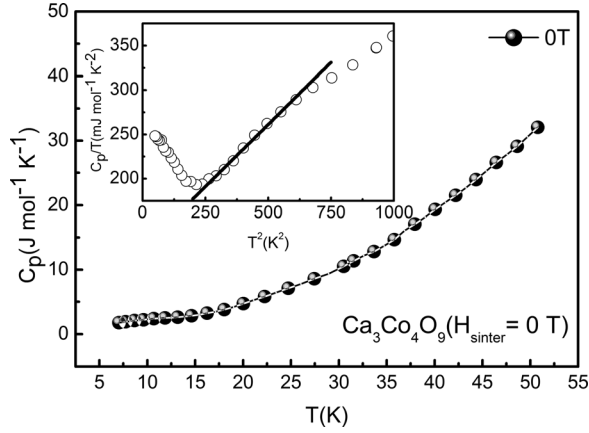
FIG. 9. Curve of $C = \gamma T + \beta T^3$ vs T for the 0 T sample. The inset shows the temperature dependence of the specific heat C in a low-temperature range via the linear fitting of $C/T = \gamma + \beta T^2$.

FIG. 10. Plot of $\ln\rho_{ab}(T)$ against T^{-1} with fitted lines for the $Ca_3Co_4O_9$ samples with $H_{sinter} = 0$, 4, 8 T in the temperature range of 25–75 K.

feasible. The solid line in the inset of Fig. 9 is the fitting result according to Eq. (4) for the 0 T sample as an example. The obtained fitting parameters γ are listed in Table I for all samples. As can be seen from Table I, all of the samples have very large γ values, revealing the existence of strong electronic correlation in the system. With increasing sample sintering magnetic field, γ decreases monotonously. The obtained result indicates that the effective electron mass m^* decreases and the electronic correlation in the system weakens under the applied sintering magnetic field. These results are consistent with the resistivity analysis. The applied magnetic field in the sample fabrication process has an effect on the electronic correlation property that is similar to the high-pressure effect in the $Ca_3Co_4O_9$ system.[29] Pressure also induces a decrease of the transport coefficient A together with an increase of T^*, due to the increase of the bandwidth under pressure. Thus, the electronic correlations and effective mass are lowered by pressure, which is typical behavior of a Fermi liquid.

In order to fully explore the reason for the distinct variations in strongly correlated properties induced by applied sintering magnetic field, now we look at the low-temperature transport mechanism of the studied samples. It is believed that now the low-temperature MI transition in the $Ca_3Co_4O_9$ system is caused by the appearance of the SDW state.[5] Usually, in the SDW state, the variation of the resistivity with temperature obeys thermally activated behavior,[5,10,25] which always follows the expression

$$\frac{1}{\rho} = \mu(T) \exp\left(-\frac{E_0}{k_B T}\right), \qquad (5)$$

where $\mu(T)$ is the mobility of carriers, E_0 is the energy gap resulting from the SDW at the Fermi surface, and k_B is the Boltzmann constant. We tried to fit the low-temperature $\rho_{ab}(T)$ data using Eq. (5) and found that only the data between $\sim$25 and 70 K can be well fitted, and the fitting temperature range shifts toward the lower temperature range slightly as the sintering field increases. The fitting results are shown in Fig. 10. The obtained fitting parameter, the activation energy E_0, is 1.942, 1.898, and 1.869 meV for the samples sintered
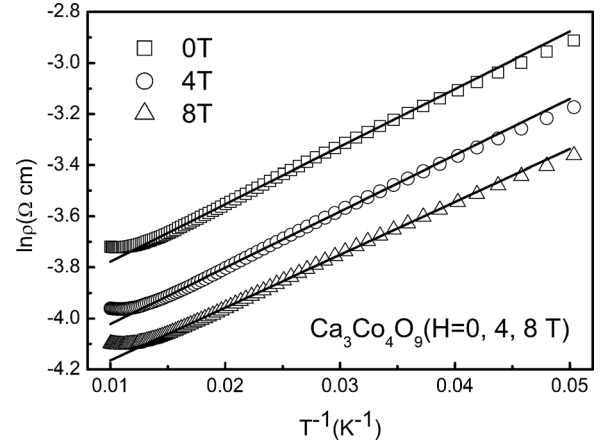
under 0, 4, and 8 T fields, respectively. E_0 decreases gradually with increasing applied magnetic field from 0 T to 8 T, implying that the applied magnetic field has a negative effect on the formation of the SDW state, as discussed in regard to temperature-dependent magnetic susceptibility behavior.

As for the low-temperature $\rho_{ab}(T)$ data below $\sim$25 K, the thermally activated mode cannot describe the data well. Instead, the Mott's two-dimensional variable range hopping (2D-VRH) model is the best one in the fitting of the curve in the temperature range of 3.5–26 K, as shown in Fig. 11. According to the variable range hopping (VRH) theory,[32] the relationship between resistivity and temperature in a 2D system can be expressed as

$$\rho(T) = \rho(0) \exp\left(\frac{T_0}{T}\right)^{1/3}, \qquad (6)$$

where $\rho(0)$ is a constant, T_0 ($= 8/[\pi k_B N(\varepsilon_F) l_\nu^2]$) is the VRH characteristic temperature associated with the density of localized states at Fermi energy $N(\varepsilon_F)$, and l_ν is the localization length.[20] As shown in Fig. 11, the linear relationship of $\ln\rho_{ab}(T)$ versus $T^{-1/3}$ indicates that the transport mechanism for all studied samples has turned into 2D-VRH in the lower temperature range. The increase of the carrier localization
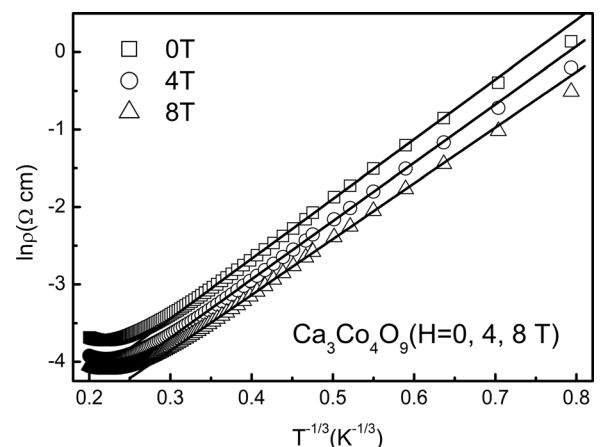

FIG. 11. Plot of $\ln\rho_{ab}(T)$ against $T^{-1/3}$ with fitted lines for the $Ca_3Co_4O_9$ samples with $H_{sinter} = 0$, 4, 8 T in the temperature range of 3.5–26 K.

with decreasing temperature might be the origin of the variation of the transport mechanism at ~25 K. The obtained fitting parameters T_0 are listed in Table I. From Table I, one can see that the value of T_0 decreases slightly with an increase of the applied sintering magnetic field, implying an increase of the localization length, which is related to the weakened localization of carriers and the enhancement of the carrier mobility. This result is contrary to that observed in the electron-doping at Ca sites in the $Ca_3Co_4O_9$ system.[7] A similar result is also observed in the Mo-doped single crystal prepared via the flux-growth method. The detailed reason for this phenomenon is under study.

Next, we try to explain the origin of the variation of the transport mechanism at ~25 K. The on-resonant spectra of x-ray photoemission spectroscopy for $Ca_3Co_4O_9$ reveals that the Co 3d partial density of states in Ca_2CoO_3 layers hardly reaches the Fermi level,[33] which indicates that Co ions in Ca_2CoO_3 layers have a very limited effect on the transport properties of the system. In contrast, the Fermi energy lies in the crystal-field gap of the d states in CoO_2 layers,[34] so Co ions in the CoO_2 layer dominate the transport behavior of the $Ca_3Co_4O_9$ system.[10] If the variation takes place in CoO_2 layers, it not only produces strong disorder and distortion in the sample but also changes the transport mechanism, because the conduction path in the CoO_2 layer is disturbed.[20] In the low-temperature range, the hole hopping tends toward farther low-energy sites rather than neighbor sites, and consequently the VRH mechanism dominates the transport behavior in the present samples. Moreover, due to the anisotropic layered structure, the VRH transport is two-dimensional. It should be emphasized that the VRH mechanism can be achieved only when the thermally activated energy is not large enough to make holes hopping to near neighbor sites, so that the VRH mechanism is first located in the lower temperature range. As the temperature increases, the holes have high enough energy, and the transport mechanism changes from VRH to the thermal activated model.[20] That is why the plot of $\ln\rho_{ab}(T)$ versus $T^{-1/3}$ in $Ca_3Co_4O_9$ samples stays linear well in the low-temperature region below ~25 K, but the linear relationship of $\ln\rho_{ab}(T)$ versus T^{-1} gradually dominates in the high-temperature region above ~25 K. With increasing sample sintering field, the activation energy E_0 decreases and the localization of carriers weakens gradually, so the thermal activated transport shifts to the lower temperature range.

D. Thermoelectric response

In order to test the thermoelectric properties, the temperature dependence of the thermopower $S(T)$ of the studied samples at zero magnetic field is measured from 10 to 330 K. For the thermal measurement, the thermal current flows along the directions parallel (referred to as the in-plane thermopower S_{ab}) and perpendicular (referred to as the out-of-plane thermopower S_c) to the pressed surface of the studied samples. Figure 12 shows the temperature dependence of the in-plane thermopower $S_{ab}(T)$ for three studied samples. The thermopower of all the samples shows a positive value in the whole measured temperature range, indicating p-type
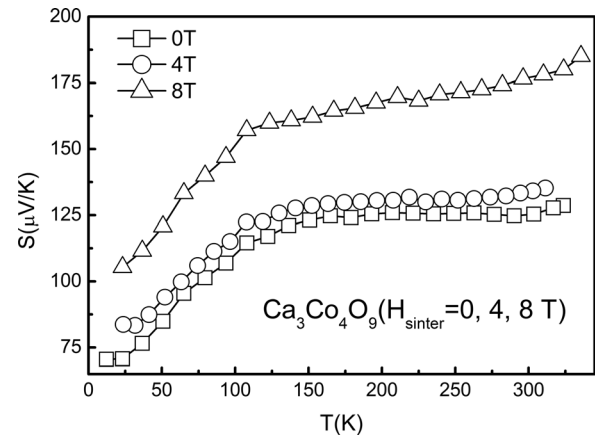

FIG. 12. Temperature dependence of the in-plane thermopower $S_{ab}(T)$ for the $Ca_3Co_4O_9$ samples with $H_{sinter} = 0$, 4, and 8 T.

conductive transport behavior. For the 0 T sample $Ca_3Co_4O_9$, Fig. 12 shows that S decreases slowly with decreasing temperature down to about ~130 K, and then S decreases rapidly as the temperature decreases from 130 K, with a variation in the slope of the $S(T)$ curve near 50 K. As the temperature decreases further from 23 K, S decreases slowly again. The room-temperature thermopower of the 0 T sample is about 125 μV/K, which agrees with findings reported earlier.[10] The larger room-temperature thermopower is usually suggested to be attributed to the degeneracy of electronic states of Co^{3+} and Co^{4+} ions and the ratio between them. Compared with the 0 T sample, the applied magnetic field in the sample sintering process does not alter the shape of the $S(T)$ curve on the whole but changes the value of S considerably. The room-temperature thermopower increases from 125.2 μV/K for the 0 T sample to 133.8 and 177.7 μV/K for the samples sintered under 4 and 8 magnetic fields, respectively. A relatively large enhancement of the thermopower has also been observed in $Ca_3Co_4O_9$ samples prepared by the as-sintered and MA + SPS annealed method,[18] in which the increased thermopower is suggested to originate from the variation of the oxygen deficiency δ in the samples. The room-temperature thermopower reaches about 160 μV/K in the sample with the oxygen deficiency δ ($= 0.083$). Compared to the $Ca_3Co_4O_9$ sample prepared via the SPS method, the thermopower S obtained by high-magnetic-field sintering in this paper is relatively large. A possible reason might be that the control of the oxygen deficiency appears only in the near-surface region of the polycrystalline sample, whereas the effect of the MA approach can reach the whole studied sample. This result indicates that the magneto-scientific approach is expected to be an effective and convenient method for the enhancement of thermopower and thus the optimization of TE performance for $Ca_3Co_4O_9$ material.

Figures 13 shows the temperature dependence of the out-of-plane thermopower $S_c(T)$ for the samples sintered under applied magnetic fields of 0, 4, and 8 T, respectively. In order to clarify, the $S_{ab}(T)$ curves are also plotted in the figures. The values of both $S_{ab}(T)$ and $S_c(T)$ are positive, implying that the major carriers in the $Ca_3Co_4O_9$ system are holes. Similar to the susceptibility and resistivity properties mentioned earlier, Fig. 13 shows that the thermopower properties of these
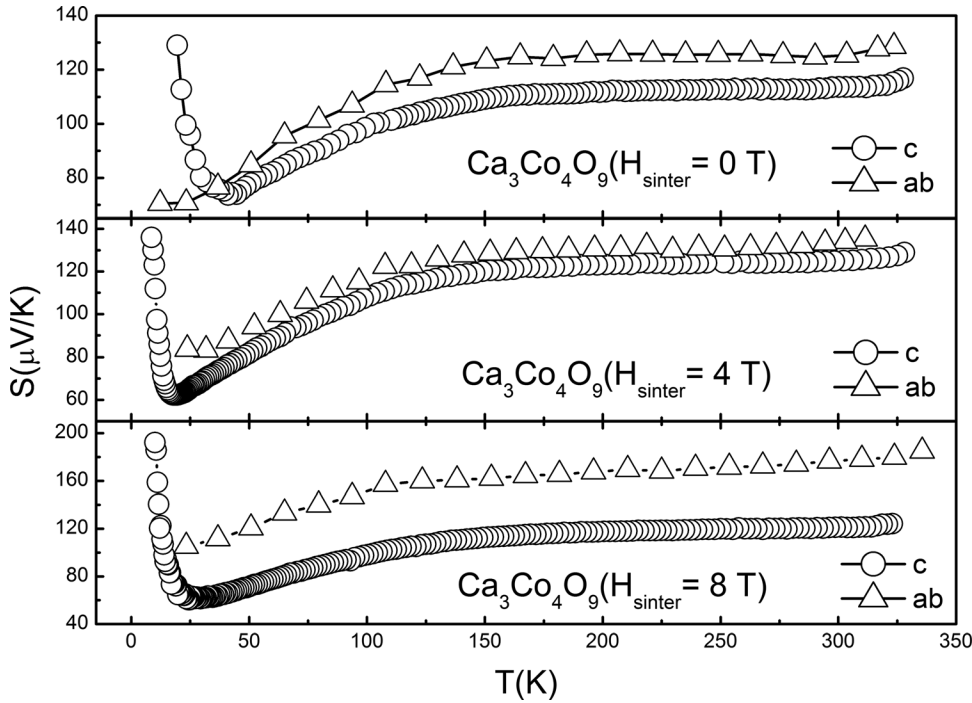
FIG. 13. Temperature dependence of the in-plane $S_{ab}(T)$ and out-of-plane $S_c(T)$ thermopower of the $Ca_3Co_4O_9$ samples with $H_{sinter} = 0$, 4, and 8 T.

samples are also anisotropic. In the high-temperature range above $T_{S\min}$ (~40 K), the $S_c(T)$ curve of the 0 T $Ca_3Co_4O_9$ sample has a temperature dependence similar to $S_{ab}(T)$, whereas its magnitude is much smaller than that of $S_{ab}(T)$. At temperatures higher than 150 K, the $S_c(T)$ curve shows weak temperature dependence. In the low-temperature range below about ~40 K, the temperature-dependence behavior of $S_c(T)$ becomes more complicated. For all the studied samples, $S_c(T)$ shows a distinct minimum at $T_{S\min}$. As the temperature decreases from $T_{S\min}$, the magnitude of the out-of-plane thermopower increases rapidly. Moreover, the upturn becomes steeper and $T_{S\min}$ moves toward lower temperatures for the $Ca_3Co_4O_9$ samples fabricated under high magnetic field. The values of $T_{S\min}$ are listed in Table I. In general, the upturn of the low-temperature out-of-plane thermopower of the $Ca_3Co_4O_9$ system is suggested to have arisen from the spin fluctuation of the system, similar to the heavy fermions and/or valence-fluctuation systems.[25,35]

In the following, we try to explain the mechanism of the large enhancement of thermopower for the samples sintered under high magnetic field. In a strong correlated system, the thermopower can be expressed by using the modified Heikes formula in the high-temperature limit,[15,36]

$$S = -\frac{k_B}{e} \ln\left[\frac{g_3}{g_4}\left(\frac{x}{1-x}\right)\right], \qquad (7)$$

where g_3 and g_4 are the spin-orbital degeneracy for Co^{3+} and Co^{4+} ions in the CoO_2 layers, respectively, x is the Co^{4+} concentration in these layers, and k_B is the Boltzmann constant. The magnetic analysis shows that the Co^{4+} concentration in the samples sintered under high magnetic field does not vary from that of the 0 T sample. That is to say, the value of x in Eq. (7) remains unchanged. The enhancement of the thermopower of the high-magnetic-field sintered samples might originate from the variation of the degeneracy of Co ions. X-ray

absorption and x-ray photoemission spectroscopy studies of $Ca_3Co_4O_9$ showed that CoO_2 layers have the low-spin (LS) configuration t_{2g}^6 for Co^{3+} and the LS configuration t_{2g}^5 for Co^{4+}, and the degeneracy of the two kinds of ions is 1 and 6,[15,37] respectively. According to the analysis of the magnetic properties, the value of the effective magnetic moment μ_{eff} and the spin quantum number s obtained from the c-axis susceptibility curves of polycrystalline samples both increase with increasing applied sintering magnetic field from 0 T to 8 T, as shown in Table I. The higher values of μ_{eff} and s in the samples sintered under high magnetic field indicate that Co ions in these samples have the higher spin state. This result shows that that the applied sintering magnetic field can change the LS state of Co^{3+} or/and Co^{4+} ions to a higher state.[38,39]

The enhancement of the thermopower in the present work can be understood qualitatively by the variation of the spin-orbital degeneracy for Co^{3+} and Co^{4+} ions due to the high-magnetic-field sintering. For Co^{3+} and Co^{4+} ions in CoO_2 layers, the spin-orbital degeneracies g_3 and g_4 are determined by the parameters Δ, K, and T, where Δ is the crystal-field splitting energy and K is the Hund's rule coupling energy.[40] Δ and K are two key parameters in determining the spin states of Co^{3+} and Co^{4+} ions in layered cobaltites. Isolated Co^{3+} and Co^{4+} ions without crystal field have high-spin (HS) states with $s = 2$ and $5/2$ due to the coupling K.[40] Introducing the octahedral crystal field Δ, the energies of the LS and intermediate-spin (IS) states decrease compared with that of the HS state, and the LS state has the lowest energy in the system.[40] Moreover, The magnitude of Δ, which gives the level crossing between HS and LS states in d^6 configurations of a Co^{3+} ion (Δ_3), is smaller than that of d^5 configurations of a Co^{4+} ion (Δ_4).[40] For the LS electronic configurations of Co^{3+} ($s = 0$), because there is only one possible way for six electrons to occupy three t_{2g} orbits, the degeneracy g_3 of Co^{3+} (LS, $s = 0$) is 1. Similarly, for the LS electronic configurations of Co^{4+} (LS, $s = 1/2$), because there are six ways for five

electrons to occupy three t_{2g} orbits, the degeneracy g_4 of Co^{4+} (LS, $s = 1/2$) is 6. The ratio of g_3 to g_4 is 1/6. When the sample is sintered under high magnetic field, the external magnetic field energy is added and competes with the crystal-field splitting energy and Hund's coupling energy in the system. Partial electrons in t_{2g} orbits obtain enough additional magnetic field energy to jump to the higher e_g orbits. In general, Co^{3+} ions are in the LS state and Co^{4+} ions are magnetic in layered cobaltites; the electron jump induced by the addition of magnetic field energy can easily occur in Co^{4+} ions. As a result, the spin-states in the samples sintered under high magnetic field are LS for Co^{3+} and LS + HS for Co^{4+}. As the sintering field increases, the average number of degeneracy of Co^{4+} ions g_4 in the system increases, and then the thermopower of the sample increases according to Eq. (7).

Next, we try to calculate the number of the spin-orbital degeneracy of Co ions in the system based on the experimental value of the thermopower, which is shown in Table II. In the following, we consider several cases (as listed in Table II) for the degeneracies: (i) For the 0 T sample, the LS states of both Co^{3+} and Co^{4+} ions are stable, and g_3 and g_4 are 1 and 6, respectively. The calculated Co^{4+} concentration x in the system is about 0.58. (ii) An applied 4 T magnetic field can excite Co^{4+} ions of partial LS Co^{4+} sites to a HS state to form a mixed spin state of LS + HS at partial Co^{4+} sites; the concentration y of the mixed state is estimated as 10.4% based on the measured thermopower value. Hence, the LS states of all Co^{3+} sites and 89.6% of Co^{4+} sites in this sample are stable. In this case, the LS and HS states of 10.4% Co^{4+} sites are close in energy and in favor of a larger degeneracy in the sample. The calculated average values of g_3 and g_4 are 1 and 6.626 for Co^{3+} and Co^{4+} ions, respectively. (iii) As the sintering magnetic field increases, Co^{4+} ions of more LS Co^{4+} sites are excited to a HS state to form the mixed LS + HS state. The concentration y of the mixed state reaches about 84.0% in the 8 T sample, and the calculated average values of g_3 and g_4 are 1 and 11.039 for Co^{3+} and Co^{4+} ions, respectively. (iv) Then we can assume that when the sintering magnetic field increases further, Co^{4+} ions of all LS Co^{4+} sites are excited to the mixed LS + HS state, the average number of the degeneracy of Co^{4+} ions should be 12, and the largest thermopower (which is 185.2 μV/K) can be reached according to the discussion by Koshibae *et al.*[40] The detailed results obtained from the discussion above are summarized in Table II. The main idea is that the applied sample sintering magnetic field can introduce an increase of

TABLE II. The ratios g_3/g_4 and the concentrations of the mixed spin state LS + HS y in Eq. (7) in cases (i)–(iv) for $Ca_3Co_4O_9$ ceramics sintered under applied magnetic fields of 0, 4, and 8 T. The obtained values of the thermopower Q at $x = 0.58$ are also presented.

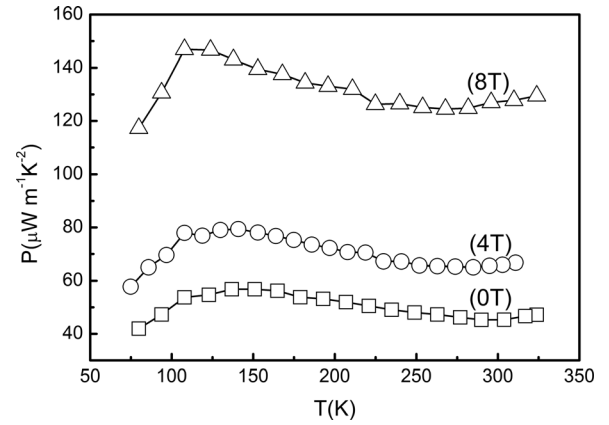| Case	H_{sinter}, T	Co^{3+}	Co^{4+}	g_3/g_4	y, %	Q, μV/K ($x = 0.58$)
i	0	LS	LS	1/6	0	125.2
ii	4	LS	LS + (LS + HS)	1/6.626	10.4	133.8
iii	8	LS	LS + (LS + HS)	1/11.039	84.0	177.7
iv	>8	LS	(LS + HS)	1/12	100	185.2

FIG. 14. Temperature dependence of the power factor ($P = S^2/\rho$) for the $Ca_3Co_4O_9$ ($H_{sinter} = 0, 4, 8$ T) samples.

the spin-orbital degeneracy of Co^{4+} ions, and thus the thermopower is enhanced for the sample sintered under high magnetic field.

In the present work, the applied sample sintering magnetic field can cause the simultaneous increase of the electric conductivity σ and the thermopower S and result in a significant increase of the power factor P ($= S^2\sigma$) for $Ca_3Co_4O_9$ samples, which is a characteristic parameter for TE material. The temperature dependence of the power factor for the studied samples is shown in Fig. 14. The power factor P at 300 K reaches 127.3 μWm^{-1} K^{-2} for the 8 T sample, which is about 1.7 times larger than that of the 0 T sample; this is also listed in Table I.

As discussed above, the applied sintering high magnetic field enhances the thermopower observably in our studied samples. However, for c-axis oriented manganese silicide fabricated with a high magnetic field, the thermopower shows values similar to that of the nonoriented specimen fabricated without high magnetic field.[16] Now we try to discuss the different effects of applied high magnetic field on the thermopower of oriented samples. For the latter, the high magnetic field is applied as the post-treatment in the progress of sample fabrication, and only affects the orientation of crystal grains, having little effect on the nucleation and growing progress. So high magnetic field has a limited effect on the thermopower and thus TE properties of the oriented sample. Nevertheless, in this paper, we apply a high magnetic field in the progress of sample sintering, which can influence the crystal nucleation and thus the spin-fluctuation in the nature to induce variation of the spin-orbital degeneracy for Co^{3+} and Co^{4+} ions. As is well known, nucleation and crystal growing are two very important stages and can influence the microstructure and performance of material directly. Thus, applying high magnetic field during the progress of crystal nucleation can enhance the thermopower and the power factor observably and thus improve the TE properties in our studied samples.

E. Thermal transport property

In the following, we pay attention to the effect of sample sintering field on the thermal transport properties of the $Ca_3Co_4O_9$ system. Figure 15 shows the temperature

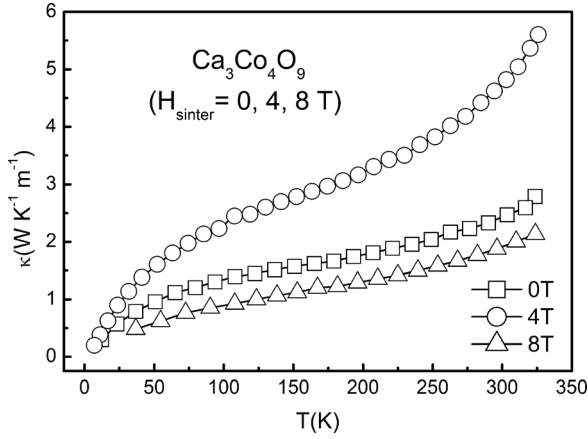FIG. 15. Temperature dependence of the in-plane thermal conductivity κ_{ab} for the Ca$_3$Co$_4$O$_9$ ($H_{sinter} = 0, 4, 8$ T) samples.

dependence of the in-plane thermal conductivity κ_{ab} for the studied samples. Similar to the magnetic, resistivity, and thermopower results, the applied sintering magnetic field does not change the $\kappa_{ab}(T)$ behavior obviously. $\kappa_{ab}(T)$ for all samples increases monotonically with increasing temperature in the whole studied temperature range. Figure 15 shows that κ_{ab} increases significantly for the 4 T sample compared to the 0 T sample, whereas κ_{ab} decreases for the 8 T sample. The room temperature κ_{ab} increases from 2.43 WK^{-1} m^{-1} for the 0 T sample to 4.75 WK^{-1} m^{-1} for the 4 T sample, but it decreases to 1.91 WK^{-1} m^{-1} for the 8 T sample. In general, the thermal conductivity in a paramagnetic material can be expressed by the sum of the phonon thermal conductivity component κ_{ph} and the carrier thermal conductivity component κ_{ch} as[2]

$$\kappa = \kappa_{ph} + \kappa_{ch}, \qquad (8)$$

where the value of κ_{ch} can be calculated from the Wiedemann-Franz law, which relates κ_{ch} to ρ as $\kappa_{ch} = LT/\rho$. In that formula, L is the Lorentz number (2.45×10^{-8} V^2 K^{-2} for free electrons) and T is the Kelvin temperature. From the calculation result, κ_{ch} in the present samples is about 10% of the total thermal conductivity κ, which is also shown in Table I.[20] The calculated phonon thermal conductivity from both the formula $\kappa_{ph} = \kappa - \kappa_{ch}$ and $\kappa_{ph} = D \times C_p \times d$ are almost the same; the phonon component κ_{ph} reaches 90% of the total thermal conductivity κ for all samples. In the latter formula $\kappa_{ph} = D \times C_p \times d$, d is the density of the specimen, D is the thermal diffusivity, and C_p is the specific heat of the samples.[19] Thereafter, the contribution of κ_{ch} to the total κ is quite small, and the phonon thermal conductivity is the main source of the total thermal conductivity in present studied samples. So, the variation of κ with the change of the sample sintering magnetic field mainly originates from the variation of κ_{ph}.[10]

According to the results of the SEM and XRD measurements and the analysis of the resistivity, the sizes of the crystal grains fabricated under high magnetic field become more homogeneous and smaller, the alignment of the c-axis of grains in entire parts of the samples trends to the direction of the c-axis of the polycrystalline sample, and the crystal is

denser on the whole. Compared with the 0 T sample, the degree of texturization of the crystal grains increases and the phonon scattering decreases, and then the localization weakens under the applied sintering magnetic field,[7] resulting in an increase of the carrier mobility and a decrease of scattering for phonons at the boundary of grains and the defects. So the phonon transport will be enhanced, and thus κ_{ph} increases and, consequently, κ increases. However, the variation of the carrier transport and the electronic structure for Co^{4+} ions induced by applying a sintering magnetic field in the CoO$_2$ layers can produce strong disorder and distortion in the sample, as discussed for the electric transport mechanism. The phonon scattering induced by the lattice disharmony increases and then κ_{ph} decreases, leading to a decrease of the whole κ for the sample. That is to say, there exist two kinds of competing mechanism in the sample to affect κ_{ph}: the degree of texturing of crystal grains and the lattice disharmony. The effect of the lattice disharmony on κ_{ph} is weaker than that of the degree of texturing, so overall κ_{ph} and then κ increase first in the 4 T sample. For the 8 T sample, the reduction of κ_{ph} due to the lattice disharmony exceeds the increase of κ_{ph} resulting from the increased degree of texturing of the crystal grains, and thus overall κ_{ph} decreases and, consequently, κ decreases.

Finally, using the measured S, ρ, and κ, we can calculate the dimensionless TE figure of merit ZT (defined as $ZT = S^2T/\rho\kappa = \sigma S^2 T/\kappa$) of the samples, which is the characteristic parameter of TE material, as well as the power factor P ($= S^2/\rho = \sigma S^2$). The in-plane ZT value as a function of temperature for the Ca$_3$Co$_4$O$_9$ series is shown in Fig. 16. It should be noted that the 4 T compound has the smallest ZT value of the three samples. The ZT value of the 4 T sample decreases considerably due to the significant increase of the thermal conductivity under an applied 4 T field, although the weak variations of the thermopower and electric conductivity make a positive contribution to ZT. The ZT value of the 8 T sample increases notably as a result of the remarkable increase of the thermopower and electric conductivity, which is about 2.6 times larger than that of the 0 T sample at 300 K, as shown in Table I. The ZT value at 300 K of the 8 T sample reaches 0.0199, which is quite high compared to the value reported earlier. So, the fabrication of layered
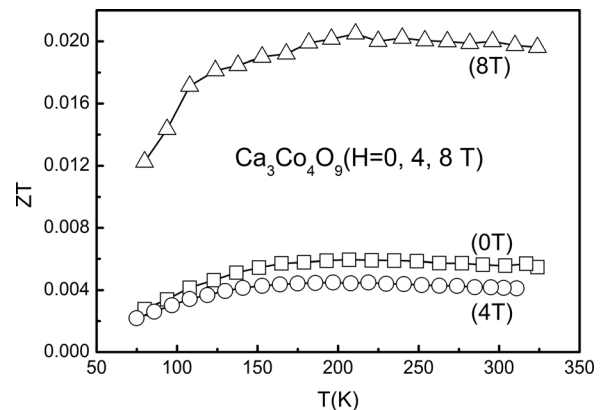

FIG. 16. Temperature dependence of the dimensionless figure of merit ZT for the Ca$_3$Co$_4$O$_9$ ($H_{sinter} = 0, 4, 8$ T) samples.

cobaltites under high magnetic field might be an effective way to improve their TE performance for high temperature applications.[25] The result shows that the applied sample sintering magnetic field can have two effects on the thermal performance of cobaltite material. The power factor increases significantly for samples sintered under high magnetic field, which is beneficial to the *ZT* value. The thermal conductivity also increases, which has a negative effect on the *ZT* value for the 4 T sample. Thus, in order to get high performance TE cobaltite material for practical usage, the applied sintering magnetic field should be high enough.

IV. CONCLUSION

Highly c-axis aligned and textured $Ca_3Co_4O_9$ samples have been fabricated via cold-pressing and then high-magnetic-field sintering methods. The effect of high-magnetic-field sintering on the structural, magnetic, electronic, and thermal transport properties has been systematically investigated. Highly textured $Ca_3Co_4O_9$ samples can be obtained via the cold-pressing method, and the degree of texturing increases monotonously with increasing sintering magnetic field. Applied sintering magnetic field makes crystal grains tend to stack along the direction of the crystalline c-axis. Two magnetic anomalies in the $d\chi(T)/dT$ versus T curve are observed for all studied samples, and are suggested to be related to the appearance of short-range spin-density-waves and a ferrimagnetic state. The in-plane resistivity of all samples shows a metal-insulator transition at T_{min}, and T_{min} decreases monotonously with increasing sintering magnetic field. All samples sintered under high magnetic field have a lower resistivity and larger thermopower than those without applied magnetic field. Moreover, the value of the resistivity decreases and the thermopower increases monotonously with increasing applied sintering magnetic field. The largest thermopower reached is 177.7 μV/*K* at 300 K under 8 T sintering field. In addition, an obvious low-temperature out-of-plane thermopower upturn is observed for all studied samples, and the upturn becomes steeper for the samples sintered under applied magnetic field. The power factor P $(=S^2/\rho)$ calculated from the in-plane resistivity and thermopower increases from 45.4 to 127.3 μWm^{-1} K^{-2} as the sintering field increases from 0 to 8 T, and the *ZT* value of the 8 T sample reaches 0.0199, which is about 2.6 times larger than that of the 0 T sample at 300 K. The obtained result is suggested to be that the applied high-magnetic-field sintering approach is an effective and convenient method for the enhancement of thermopower and thus the optimization of TE properties in $Ca_3Co_4O_9$ material.

ACKNOWLEDGMENTS

[1]J. Sugiyama, J. H. Brewer, E. J. Ansaldo, H. Itahara, K. Dohmae, Y. Seno, C. Xia, and T. Tani, Phys. Rev. B **68**, 134423 (2003).

[2]Y. Wang, Y. Sui, X. J. Wang, W. H. Su, and X. Y. Liu, J. Appl. Phys. **107**, 033708 (2010).

[3]S. Pinitsoontorn, N. Lerssongkram, A. Harnwunggmoung, K. Kurosaki, and S. Yamanaka, J. Alloys Compd. **503**, 431 (2010).

[4]Y. Wang, L. X. Xu, Y. Sui, X. J. Wang, J. G. Cheng, and W. H. Su, Appl. Phys. Lett. **97**, 062114 (2010).

[5]B. C. Zhao, Y. P. Sun, and W. H. Song, J. Appl. Phys. **99**, 073906 (2006).

[6]L. B. Wang, A. Maignan, D. Pelloquin, S. Hebert, and B. Raveau, J. Appl. Phys. **92**, 124 (2002).

[7]Y. Wang, Y. Sui, J. G. Cheng, X. J. Wang, W. H. Su, X. Y. Liu, and H. J. Fan, J. Phys. Chem. C **114**, 5174 (2010).

[8]I. Terasaki, Y. Sasago, and K. Uchinokura, Phys. Rev. B **56**, R12685 (1997).

[9]A. C. Masset, C. Michel, A. Maignan, M. Hervieu, O. Toulemonde, F. Studer, B. Raveau, and J. Hejtmanek, Phys. Rev. B **62**, 166 (2000).

[10]Y. Wang, Y. Sui, P. Ren, L. Wang, X. J. Wang, W. H. Su, and H. J. Fan, Chem. Mater. **22**, 1155 (2010).

[11]Q. Yao, D. L. Wang, L. D. Chen, X. Shi, and M. Zhou J. Appl. Phys. **97**, 103905 (2005).

[12]J. Sugiyama, H. Itahara, T. Tani, J. H. Brewer, and E. J. Ansaldo, Phys. Rev. B **66**, 134413 (2002).

[13]G. Xu, R. Funahashi, M. Shikano, I. Matsubara, and Y. Zhou, Appl. Phys. Lett. **80**, 3760 (2002).

[14]Y. Wang, Y. Sui, J. Cheng, X. Wang, J. Miao, Z. Liu, Z. Qian, and W. Su, J. Alloys Compd. **448**, 1 (2008).

[15]G. Tang, Z. Wang, X. Xu, L. Qiu, L. Xing, and Y. Du, J. Mater. Sci. **45**, 3969 (2010).

[16]H. Kaga, Y. Kinemuchi, K. Watari, S. Tanaka, A. Makiya, Z. Kato, and K. Uematsu, J. Mater. Res. **22**, 2917 (2007).

[17]I. Matsubara, R. Funahashi, T. Takeuchi, and S. Sodeoka, J. Appl. Phys. **90**, 462 (2001).

[18]M. Sano, S. Horii, I. Matsubara, R. Funahashi, M. Shikano, J. Shimoyama, and K. Kishio, Jpn. J. Appl. Phys. **42**, 198 (2003).

[19]J. Xu, C. P. Wei, and K. Jia, J. Alloys Compd. **500**, 227 (2010).

[20]J. L. Lan, Y. H. Lin, G. J. Li, S. L. Xu, Y. Liu, C. W. Nan, and S. J. Zhao, Appl. Phys. Lett. **96**, 192104 (2010).

[21]S. Li, R. Funahashi, I. Matsubara, K. Ueno, S. Sodeoka, and H. Yamada, Chem. Mater. **12**, 2424 (2000).

[22]J. Sugiyama, C. Xia, and T. Tani, Phys. Rev. B **67**, 104410 (2003).

[23]S. Horii, I. Matsubara, M. Sano, K. Fujie, M. Suzuki, R. Funahashi, M. Shikano, W. Shin, N. Murayama, J. Shimoyama, and K. Kishio, Jpn. J. Appl. Phys. **42**, 7018 (2003).

[24]C. J. Liu, L. C. Huang, and J. S. Wang, Appl. Phys. Lett. **89**, 204102 (2006).

[25]B. C. Zhao, Y. P. Sun, W. J. Lu, X. B. Zhu, and W. H. Song, Phys. Rev. B **74**, 144417 (2006).

[26]G. D. Tang, Z. H. Wang, X. N. Xu, L. Qiu, and Y. W. Du, J. Appl. Phys. **107**, 053715 (2010).

[27]W. Chen, K. Hida, and B. C. Sanctuary, Phys. Rev. B **67**, 104401 (2003).

[28]M. Shikano and R. Funahashi, Appl. Phys. Lett. **82**, 1851 (2003).

[29]P. Limelette, V. Hardy, P. Auban-Senzier, D. Jérome, D. Flahaut, S. Hebert, R. Fresard, C. Simon, J. Noudem, and A. Maignan, Phys. Rev. B **71**, 233108 (2005).

[30]P. Schiffer, A. P. Ramirez, W. Bao, and S. W. Cheong, Phys. Rev. Lett. **75**, 3336 (1995).

[31]A. Georges, G. Kotliar, W. Krauth, and M. J. Rozenberg, Rev. Mod. Phys. **68**, 13 (1996).

[32]N. F. Mott and E. A. Davis, *Electronic Processes in Non-crystalline Materials* (Clarendon, London, 1971).

[33]T. Takeuchi, T. Kondo, T. Takami, H. Takahashi, H. Ikuta, U. Mizutani, K. Soda, R. Funahashi, M. Shikano, and M. Mikami, Phys. Rev. B **69**, 125410 (2004).

[34]R. Asahi, J. Sugiyama, and T. Tani, Phys. Rev. B **66**, 155103 (2002).

[35]C. S. Garde and J. Ray, Phys. Rev. B **51**, 2960 (1995).

[36]P. M. Chaikin and G. Beni, Phys. Rev. B **13**, 647 (1976).

[37]T. Mizokawa, L. H. Tjeng, H. J. Lin, C. T. Chen, R. Kitawaki, I. Terasaki, S. Lambert, and C. Michel, Phys. Rev. B **71**, 193107 (2005).

[38]S. Hébert, S. Lambert, D. Pelloquin, and A. Maignan, Phys. Rev. B **64**, 172101 (2001).

[39]T. Mizokawa, L. H. Tjeng, P. G. Steeneken, N. B. Brookes, I. Tsukada, T. Yamamoto, and K. Uchinokura, Phys. Rev. B **64**, 115104 (2001).

[40]W. Koshibae, K. Tsutsui, and S. Maekawa, Phys. Rev. B **62**, 6869 (2000).